

Histomorphology-driven multi-instance learning for breast cancer WSI classification

Baizhi Wang^{1,2}, Rui Yan✉^{1,2}, Wenxin Ma^{1,2}, Xu Zhang^{1,2}, Yuhao Wang^{1,2},
Xiaolong Li^{1,2}, Yunjie Gu^{1,2}, Zihang Jiang^{1,2}, and S. Kevin Zhou✉^{1,2,3,4}

¹ School of Biomedical Engineering, Division of Life Sciences and Medicine,
University of Science and Technology of China (USTC)

² Center for Medical Imaging, Robotics, Analytic Computing & Learning
(MIRACLE), Suzhou Institute for Advance Research, USTC

³ Key Laboratory of Intelligent Information Processing of CAS, ICT, CAS

⁴ State Key Laboratory of Precision and Intelligent Chemistry, USTC
yanrui@ustc.edu.cn s.kevin.zhou@gmail.com

Abstract. Histomorphology is crucial in breast cancer diagnosis. However, existing whole slide image (WSI) classification methods struggle to effectively incorporate histomorphology information, limiting their ability to capture key and fine-grained pathological features. To address this limitation, we propose a novel framework that explicitly incorporates histomorphology (tumor cellularity, cellular morphology, and tissue architecture) into WSI classification. Specifically, our approach consists of three key components: (1) estimating the importance of tumor-related histomorphology information at the patch level based on medical prior knowledge; (2) generating representative cluster-level features through histomorphology-driven cluster pooling; and (3) enabling WSI-level classification through histomorphology-driven multi-instance aggregation. With the incorporation of histomorphological information, our framework strengthens the model’s ability to capture key and fine-grained pathological patterns, thereby enhancing WSI classification performance. Experimental results demonstrate its effectiveness, achieving high diagnostic accuracy for molecular subtyping and cancer subtyping. The code will be available.

Keywords: Computational Pathology · Whole Slide Images · Multiple Instance Learning · Breast Cancer.

1 Introduction

Breast cancer is the most prevalent and lethal malignancy among women. According to the global cancer observatory, breast cancer comprised 2.3 million of the 19.3 million new cancer cases in 2020, contributing to 15.5% of all cancer-related deaths in women [12]. Despite significant advances in oncology, the complexity of cancer pathogenesis and the lack of definitive cures [1] continue to drive research efforts focused on improving diagnosis, prognosis, and treatment.

Among the key histopathological factors in breast cancer diagnosis, tumor structure and tumor cellularity provide essential prognostic information. Tumor structure (cellular morphology and tissue architecture), assessed through the Nottingham Grading System (NGS) [6], evaluates tumors based on nuclear atypia, mitotic count, and tubule formation, each scored from 1 to 3, with the cumulative score determining tumor grade. This grading system is fundamental for assessing tumor structure. Tumor cellularity, defined as the proportion of the tumor bed occupied by malignant cells, is another crucial factor, particularly for estimating tumor burden and predicting treatment response [14].

Computational pathology has significantly advanced whole slide image (WSI) analysis through deep learning [3, 4, 11], with most approaches relying on the weakly supervised learning paradigm known as Multi-Instance Learning (MIL) [5, 8]. However, existing computational models often fail to explicitly incorporate tumor structure and cellularity into decision making process, limiting their ability to capture fine-grained pathological features essential for precise diagnosis and prognosis.

To overcome these limitations, we propose **HistoMorphology-Driven Multi-Instance Learning (HMDMIL)**, a novel framework designed to seamlessly integrate with existing MIL methods. This plug-and-play approach explicitly incorporates tumor structural information and tumor cellularity into the feature aggregation process. Extensive experimental results demonstrate a strong correlation between accurately capturing tumor histomorphology and improving tumor diagnosis accuracy. These findings highlight the importance of incorporating histomorphological information to enhance the clinical utility of computational pathology models.

The contributions of this paper can be summarized as follows:

- We integrate histomorphological knowledge into WSI-level classification by leveraging key medical priors such as tumor cellularity, cellular morphology, and tissue architecture. This enables the model to capture critical pathological patterns, which are essential for WSI classification.
- We propose HMDMIL, a novel and adaptable histomorphology-driven multi-instance learning framework, designed to enhance knowledge aggregation through three key components: histomorphology-centric importance estimation network, histomorphology-driven cluster pooling, and histomorphology-driven multi-instance aggregation.
- Extensive experiments demonstrate that HMDMIL is highly flexible and broadly applicable across various MIL models and downstream tasks, consistently leading to significant performance improvements.

2 Methods

The overview of HMDMIL is illustrated in Fig. 1. In addition to traditional MIL components, i.e. patch encoder, feature aggregation module, and classifier, HMDMIL contains two novel designs: Histomorphology-Centric Importance Estimation Network and Histomorphology-Driven Cluster Pooling.

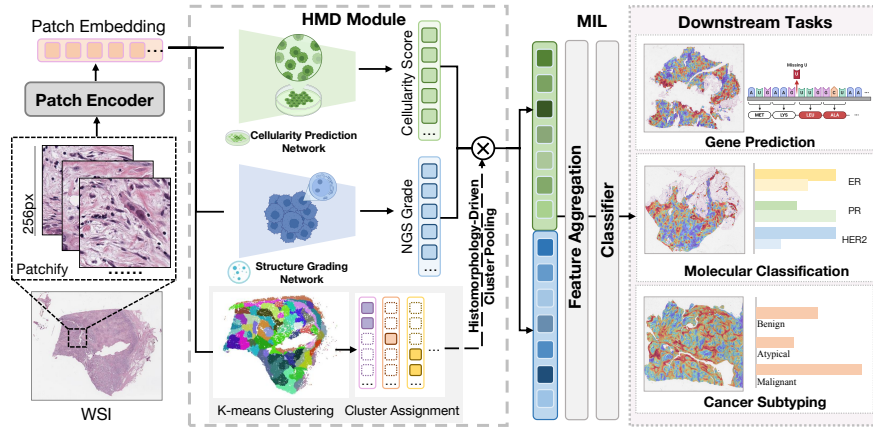


Fig. 1: Overview of HMDMIL. Given a set of patches cropped from a slide, we sequentially utilize Patch Encoder, Histomorphology-Driven Clustering, and Multi-Instance learning for WSI analysis of different downstream tasks.

To begin with, we first sample patches from a WSI, and encode them into patch embeddings:

$$X = \text{PatchEncoder}(P), \quad (1)$$

where $P \in \mathbb{R}^{N \times 3 \times 256 \times 256}$ is the input patch, and $X \in \mathbb{R}^{N \times C \times H \times W}$ is the extracted patch embedding.

Histomorphology-centric importance estimation network. Our method employs two auxiliary networks to predict the tumor cellularity and tumor structure grade of each patch, respectively. These predictions generate the importance scores for each patch, which are then used for the pooling process.

Cellularity prediction network (CPN). To estimate instance-level tumor cellularity, we developed a lightweight CPN to predict the tumor cellularity for each instance feature. The CPN is trained using the BreastPathQ dataset [10], which contains high-quality, instance-level annotations for tumor cellularity assessment. Given an input instance feature X , the cellularity score of X is computed as: $C_k = \text{CPN}(X)$, where $\text{CPN}(\cdot)$ denotes the trained CPN, and $C_k \in \mathbb{R}^{N \times C}$ represents the predicted instance-level cellularity score.

Structure grading network (SGN). Similarly, to estimate instance-level tumor structure grade, we designs a lightweight SGN to predict the NGS grade for each instance feature. The SGN was trained on the MITOS-ATYPIA-14 [15] dataset, which provides detailed annotations for histological grading. For a given input instance feature X , the structure grade is estimated as: $S_k = \text{SGN}(X)$, where $\text{SGN}(\cdot)$ is the trained SGN, and $S_k \in \mathbb{R}^{N \times C}$ denotes the predicted instance-level tumor structure grade.

Histomorphology-driven cluster pooling. Due to the significant redundancy present in WSIs, it is a typical strategy to cluster patch features and generate representative features for each cluster. Initially, we employ k-means

clustering to generate a number of clusters, from which we select several features for each cluster.

$$X_k = M_k X, \quad (2)$$

where $M_k \in \mathbb{R}^{N_k \times N}$ is a selective matrix, and N_k is the number of selected patches within the k -th cluster.

Unlike previous methods that obtain cluster-level features through simple mean averaging, our approach incorporates histomorphological knowledge from each patch, estimated by the auxiliary networks, to derive more representative cluster features.

We first utilize the estimated tumor cellularity to generate two masks, which separately corresponds to the top half patches and the bottom half within each cluster. Specifically, the top half of patches are utilized to generate positive cluster features, while the bottom half are used to derive negative cluster features. Then, we use these two masks and the instance-level tumor cellularity to obtain cluster-level representative features:

$$X_{C,k}^{pos} = Norm((M_{C,k}^{pos} \odot C_k)X_k), \quad (3)$$

$$X_{C,k}^{neg} = Norm((M_{C,k}^{neg} \odot C_k)X_k), \quad (4)$$

where $M_{C,k}^{pos}, M_{C,k}^{neg} \in \mathbb{R}^{N_k}$ mean the positive and negative cellularity patch masks of the k -th cluster, $C_k \in \mathbb{R}^{N_k}$ means the tumor cellularity, and $X_k \in \mathbb{R}^{N_k \times D}$ means the patch features.

Similarly, we employ the estimated tumor structure grade to assign an structure importance weight to each patch within a cluster, thereby generating both positive and negative representative features for each cluster:

$$X_{S,k}^{pos} = Norm((M_{S,k}^{pos} \odot S_k)X_k), \quad (5)$$

$$X_{S,k}^{neg} = Norm((M_{S,k}^{neg} \odot S_k)X_k), \quad (6)$$

where $M_{S,k}^{pos}, M_{S,k}^{neg} \in \mathbb{R}^{N_k}$ mean the positive and negative structure patch mask of the k -th cluster, $S_k \in \mathbb{R}^{N_k}$ means the tumor structure grade, and $X_k \in \mathbb{R}^{N_k \times D}$ means the patch features.

Consequently, we obtain four types of representative features for each cluster center across the entire slide. For each cluster S_k , the Histomorphology-Driven Cluster Pooling method ultimately generates four cluster features:

$$\mathcal{X}_k = \{X_{C,k}^{pos}, X_{C,k}^{neg}, X_{S,k}^{pos}, X_{S,k}^{neg}\}. \quad (7)$$

Histomorphology-driven multi-instance aggregation. The cluster features obtained through histomorphology-driven cluster pooling can be seamlessly integrated into various MIL frameworks.

In MIL, the training dataset consists of multiple clusters, each assigned a label, while the individual instances within a cluster remain unlabeled. The cluster’s label is determined by the presence of positive instances: if at least one instance in a cluster is positive, the entire cluster is labeled as positive; if all

instances are negative, the cluster is classified as negative. The feature aggregation module is essential in this process, as it integrates instance-level features to generate cluster-level predictions. Given an instance x_d and corresponding label $y_d \in \{0, 1\}$ in a cluster $B = \{(x_1, y_1), \dots, (x_D, y_D)\}$, the label of B is given by:

$$Y = \prod_{d=1}^D y_d = \begin{cases} 0, & \forall y_d = 0 \\ 1, & \exists y_d = 1 \end{cases} \quad (8)$$

Subsequently, the WSI-level feature representation is fed into different classifiers to perform different downstream tasks, e.g., molecular subtyping and cancer subtyping.

3 Experiments

3.1 Datasets and evaluation metrics

We focus on two tasks: *Molecular Subtyping* and *Cancer Subtyping*. For the former, we perform experiments on estrogen receptor (ER), progesterone receptor (PR), and human epidermal growth factor receptor 2 (HER2) classification using datasets from TCGA-BRCA [17] and BCNB [18]. For the latter, We perform extensive experiments on two public datasets: BRACS [2] and TCGA-BRCA.

To mitigate the impact of data partitioning on model evaluation, we employ 5-fold cross-validation. For performance evaluation, we adopt the Area Under the ROC Curve (AUC) and Accuracy (ACC) metrics, along with their standard deviation (std), following standard practice.

3.2 Implementation details

To evaluate the effectiveness of **HistoMorphology-Driven** (HMD) design, we compare it against several state-of-the-art methods, including conventional pooling methods such as Mean Pooling and Max Pooling, attention-based multiple instance learning (ABMIL [8]) and its variants CLAM-SB [9], as well as Transformer-based approaches like TransMIL [16]. Additionally, we evaluate SSM-based S4MIL [7] and the Mamba-based MambaMIL [21] model. To ensure fair comparisons, the patch embedding are extracted using the Gigapath [19] tile encoder, whose structure is ViT-G/14 model and pre-trained with DINOv2 [13] method. We adopt the same data preprocessing pipeline as Gigapath. Following HDMIL [20], we select $K=50$ as the number of clusters.

3.3 Comparison results

Molecular subtyping. As shown in Table 1, we investigate the impact of HMD on ER, PR, and HER2 classification using the TCGA-BRCA and BCNB datasets. The results demonstrate that integrating HMD leads to performance improvements across nearly all baseline models. The most significant enhancement is observed in MambaMIL, where HMD improves classification performance

Table 1: Molecular Subtyping Results on TCGA-BRCA and BCNB Datasets

TCGA-BRCA								
Method	ER		PR		HER2		Mean	
	AUC	ACC	AUC	ACC	AUC	ACC	AUC	ACC
Mean Pooling	0.888±0.041	0.835±0.037	0.842±0.050	0.799±0.067	0.751±0.048	0.835±0.029	0.827	0.823
+HMD(ours)	0.890±0.047	0.842±0.049	0.842±0.048	0.805±0.062	0.753±0.047	0.843±0.028	0.828	0.83
Max Pooling	0.811±0.070	0.802±0.050	0.828±0.055	0.776±0.063	0.718±0.058	0.819±0.027	0.785	0.799
+HMD(ours)	0.861±0.041	0.841±0.060	0.830±0.050	0.785±0.059	0.759±0.041	0.823±0.048	0.816	0.816
TransMIL	0.853±0.041	0.806±0.062	0.794±0.051	0.750±0.059	0.710±0.089	0.830±0.048	0.785	0.795
+HMD(ours)	0.863±0.062	0.806±0.052	0.838±0.056	0.760±0.050	0.683±0.093	0.832±0.065	0.794	0.799
MambaMIL	0.867±0.035	0.828±0.047	0.829±0.070	0.783±0.073	0.749±0.027	0.839±0.060	0.815	0.816
+HMD(ours)	0.881±0.030	0.830±0.038	0.866±0.082	0.808±0.060	0.755±0.072	0.846±0.018	0.834	0.828
attMIL	0.851±0.059	0.805±0.059	0.843±0.067	0.793±0.095	0.783±0.030	0.815±0.024	0.825	0.804
+HMD(ours)	0.859±0.061	0.826±0.091	0.862±0.055	0.812±0.050	0.797±0.018	0.815±0.021	0.839	0.817
CLAM-SB	0.870±0.055	0.843±0.066	0.854±0.065	0.814±0.065	0.747±0.038	0.799±0.039	0.823	0.818
+HMD(ours)	0.870±0.035	0.834±0.051	0.865±0.057	0.808±0.045	0.767±0.052	0.838±0.065	0.834	0.826
S4MIL	0.871±0.026	0.834±0.040	0.859±0.067	0.797±0.059	0.772±0.055	0.844±0.051	0.834	0.825
+HMD(ours)	0.868±0.023	0.814±0.037	0.865±0.067	0.803±0.076	0.782±0.022	0.836±0.040	0.838	0.817
BCNB								
Method	ER		PR		HER2		Mean	
	AUC	ACC	AUC	ACC	AUC	ACC	AUC	ACC
Mean Pooling	0.891±0.054	0.847±0.046	0.813±0.041	0.796±0.030	0.701±0.062	0.730±0.041	0.801	0.791
+HMD(ours)	0.895±0.056	0.840±0.043	0.820±0.039	0.800±0.027	0.703±0.071	0.731±0.081	0.806	0.79
Max Pooling	0.893±0.055	0.852±0.053	0.805±0.043	0.775±0.033	0.671±0.045	0.715±0.039	0.789	0.78
+HMD(ours)	0.894±0.046	0.839±0.047	0.807±0.037	0.792±0.041	0.700±0.059	0.731±0.064	0.800	0.787
TransMIL	0.859±0.040	0.859±0.040	0.757±0.025	0.677±0.108	0.680±0.046	0.679±0.088	0.765	0.738
+HMD(ours)	0.867±0.035	0.828±0.020	0.783±0.020	0.777±0.056	0.684±0.052	0.713±0.041	0.778	0.772
MambaMIL	0.894±0.023	0.828±0.031	0.783±0.026	0.779±0.039	0.674±0.053	0.707±0.038	0.783	0.771
+HMD(ours)	0.911±0.044	0.858±0.046	0.816±0.017	0.803±0.027	0.690±0.058	0.713±0.047	0.805	0.791
ABMIL	0.914±0.037	0.845±0.060	0.821±0.025	0.777±0.039	0.703±0.072	0.728±0.036	0.812	0.783
+HMD(ours)	0.916±0.035	0.864±0.043	0.827±0.017	0.785±0.036	0.736±0.058	0.728±0.043	0.826	0.792
CLAM-SB	0.899±0.053	0.850±0.559	0.794±0.040	0.783±0.044	0.697±0.067	0.720±0.063	0.796	0.784
+HMD(ours)	0.908±0.035	0.854±0.039	0.792±0.045	0.790±0.047	0.709±0.071	0.743±0.043	0.803	0.795
S4MIL	0.898±0.037	0.847±0.027	0.823±0.0225	0.794±0.012	0.708±0.046	0.735±0.027	0.809	0.792
+HMD(ours)	0.901±0.046	0.858±0.053	0.823±0.033	0.790±0.039	0.719±0.055	0.737±0.030	0.814	0.795

by 1.9% in AUC and 1.2% in ACC on the TCGA-BRCA dataset, and by 2.2% in AUC and 2.0% in ACC on the BCNB dataset. These findings further highlight the effectiveness of HMD, particularly in Mamba-based architectures.

Cancer subtyping. As shown in Table 2, we investigate the impact of HMD on cancer subtyping using the BRACS and TCGA-BRCA datasets. Consistently, the results demonstrate that integrating HMD leads to performance improvements across nearly all baseline models. The most significant enhancement is observed in ABMIL, where HMD improves classification performance by 1.2% in AUC and 0.5% in ACC. These findings highlight the effectiveness of HMD in attention-based architectures, improving cancer subtyping performance.

Overall, HMDMIL exhibits consistently stable performance across all evaluated MIL methods, highlighting its strong capability in aggregating instance features. This improvement stems from discriminative representations extracted from tumor cellularity and tumor structure information at the instance level.

Table 2: Cancer Subtyping Results on BRACS and TCGA-BRCA Datasets

Cancer Subtyping								
Method	BRACS-7		BRACS-3		TCGA-BRCA-2		Mean	
	AUC	ACC	AUC	ACC	AUC	ACC	AUC	ACC
Mean Pooling	0.788±0.053	0.471±0.109	0.857±0.020	0.701±0.028	0.877±0.030	0.849±0.063	0.840	0.673
+HMD(ours)	0.789±0.053	0.475±0.109	0.857±0.020	0.702±0.024	0.877±0.030	0.851±0.059	0.841	0.676
Max Pooling	0.784±0.031	0.505±0.041	0.847±0.035	0.724±0.054	0.873±0.050	0.845±0.034	0.834	0.691
+HMD(ours)	0.808±0.039	0.513±0.052	0.855±0.031	0.742±0.049	0.878±0.047	0.851±0.057	0.847	0.702
TransMIL	0.789±0.044	0.460±0.021	0.875±0.045	0.743±0.057	0.883±0.033	0.851±0.028	0.849	0.684
+HMD(ours)	0.798±0.032	0.462±0.054	0.878±0.026	0.732±0.045	0.887±0.042	0.856±0.039	0.854	0.683
mambaMIL	0.831±0.035	0.513±0.067	0.888±0.043	0.721±0.025	0.873±0.071	0.825±0.035	0.864	0.686
+HMD(ours)	0.822±0.037	0.468±0.047	0.901±0.020	0.762±0.047	0.871±0.007	0.810±0.059	0.864	0.680
ABMIL	0.835±0.037	0.520±0.063	0.895±0.026	0.751±0.062	0.901±0.022	0.862±0.021	0.877	0.711
+HMD(ours)	0.839±0.030	0.524±0.055	0.899±0.039	0.777±0.084	0.901±0.018	0.876±0.021	0.879	0.725
CLAM-sb	0.840±0.040	0.543±0.043	0.872±0.036	0.743±0.047	0.905±0.009	0.870±0.018	0.872	0.718
+HMD(ours)	0.845±0.028	0.554±0.010	0.902±0.039	0.743±0.049	0.905±0.013	0.872±0.014	0.884	0.723
S4MIL	0.827±0.031	0.520±0.059	0.904±0.024	0.773±0.040	0.895±0.018	0.860±0.030	0.875	0.717
+HMD(ours)	0.844±0.037	0.547±0.055	0.897±0.036	0.735±0.042	0.899±0.015	0.874±0.020	0.880	0.718

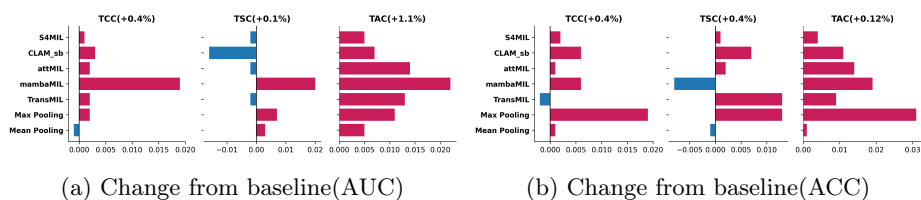


Fig. 2: Ablation experiments on different components

3.4 Ablation study

To evaluate the effectiveness of HMDMIL, we perform an ablation study comparing the performance of its two key components: Tumor Cellularity Cluster (TCC) and Tumor Structure Cluster (TSC). To ensure a fair evaluation of each component, we maintain identical training settings across all experiments.

As illustrated in Fig. 2, in molecular subtyping tasks, TCC improves the AUC by an average of 0.4% across various MIL methods, while TSC yields an average improvement of 0.2%. When combined, HMDMIL achieves a more substantial enhancement, with an average AUC increase of 1.1% across different MIL approaches. These results demonstrate that both TCC and TSC contribute positively to molecular subtyping tasks within MIL frameworks, validating their effectiveness in improving model performance. We also perform visualizations to illustrate the effectiveness of our proposed method. Fig. 3 shows UMAP visualization of slide embeddings in BRACS, color-coded by different cancer types for visual decluttering. Fig. 4 and Fig. 5 shows different distributions of histomorphology-driven importance scores and attention weights.

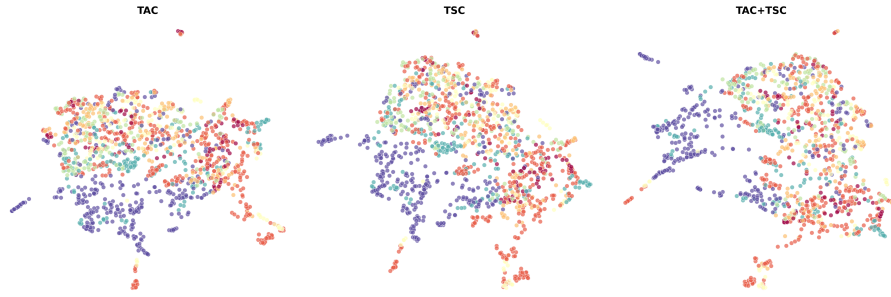


Fig. 3: UMAP visualization of slide embedding spaces for BRACS

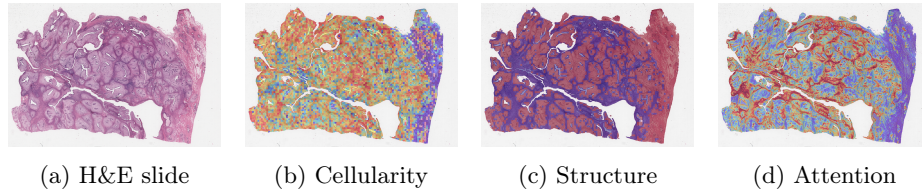


Fig. 4: Visualization of histomorphology-driven importance scores for BRACS

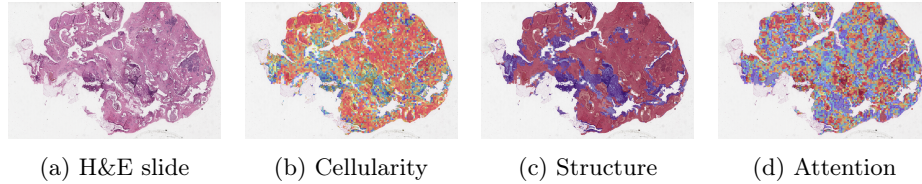


Fig. 5: Visualization of histomorphology-driven importance scores for TCGA

4 Conclusions

This paper presents HMDMIL, a novel framework for incorporating tumor histomorphology information into MIL models. HMDMIL leverages two pretrained neural networks to predict tumor structure grade and tumor cellularity, which guide the clustering of instance-level features. A histomorphology-driven cluster pooling mechanism then aggregates these features into cluster-level features, effectively integrating tumor histomorphology into the MIL framework. Experimental results demonstrate the effectiveness and generalizability of HMDMIL across various MIL-based models, while ablation studies confirm that incorporating tumor structure and cellularity enhances performance.

Compared to existing methods, our proposed approach is both flexible and versatile, seamlessly integrating with various MIL models and consistently enhancing performance across different downstream tasks. These advantages estab-

lish HMDMIL as a promising framework for MIL-based WSI analysis, improving both model interpretability and diagnostic accuracy.

References

1. Blackadar, C.B.: Historical review of the causes of cancer. *World journal of clinical oncology* **7**(1), 54 (2016)
2. Brancati, N., Anniciello, A.M., Pati, P., Riccio, D., Scognamiglio, G., Jaume, G., De Pietro, G., Di Bonito, M., Foncubierta, A., Botti, G., et al.: Bracs: A dataset for breast carcinoma subtyping in h&e histology images. *Database* **2022**, baac093 (2022)
3. Campanella, G., Hanna, M.G., Geneslaw, L., Mirafior, A., Werneck Krauss Silva, V., Busam, K.J., Brogi, E., Reuter, V.E., Klimstra, D.S., Fuchs, T.J.: Clinical-grade computational pathology using weakly supervised deep learning on whole slide images. *Nature medicine* **25**(8), 1301–1309 (2019)
4. Chen, R., Yang, L., Goodison, S., Sun, Y.: Deep-learning approach to identifying cancer subtypes using high-dimensional genomic data. *Bioinformatics* **36**(5), 1476–1483 (2020)
5. Courtiol, P., Tramel, E.W., Sanselme, M., Wainrib, G.: Classification and disease localization in histopathology using only global labels: A weakly-supervised approach. *arXiv preprint arXiv:1802.02212* (2018)
6. Elston, C.W., Ellis, I.O.: Pathological prognostic factors in breast cancer. i. the value of histological grade in breast cancer: experience from a large study with long-term follow-up. *Histopathology* **19**(5), 403–410 (1991)
7. Fillioux, L., Boyd, J., Vakalopoulou, M., Cournède, P.H., Christodoulidis, S.: Structured state space models for multiple instance learning in digital pathology. In: *International Conference on Medical Image Computing and Computer-Assisted Intervention*. pp. 594–604. Springer (2023)
8. Ilse, M., Tomczak, J., Welling, M.: Attention-based deep multiple instance learning. In: *International conference on machine learning*. pp. 2127–2136. PMLR (2018)
9. Lu, M.Y., Williamson, D.F., Chen, T.Y., Chen, R.J., Barbieri, M., Mahmood, F.: Data-efficient and weakly supervised computational pathology on whole-slide images. *Nature biomedical engineering* **5**(6), 555–570 (2021)
10. Martel, A., Nofech-Mozes, S., Salama, S., Akbar, S., Peikari, M.: Assessment of residual breast cancer cellularity after neoadjuvant chemotherapy using digital pathology [data set]. *The Cancer Imaging Archive* (2019)
11. Mobadersany, P., Yousefi, S., Amgad, M., Gutman, D.A., Barnholtz-Sloan, J.S., Velázquez Vega, J.E., Brat, D.J., Cooper, L.A.: Predicting cancer outcomes from histology and genomics using convolutional networks. *Proceedings of the National Academy of Sciences* **115**(13), E2970–E2979 (2018)
12. Nolan, E., Lindeman, G.J., Visvader, J.E.: Deciphering breast cancer: from biology to the clinic. *Cell* **186**(8), 1708–1728 (2023)
13. Oquab, M., Darcet, T., Moutakanni, T., Vo, H., Szafraniec, M., Khalidov, V., Fernandez, P., Haziza, D., Massa, F., El-Nouby, A., et al.: Dinov2: Learning robust visual features without supervision. *arXiv preprint arXiv:2304.07193* (2023)
14. Rajan, R., Poniecka, A., Smith, T.L., Yang, Y., Frye, D., Pusztai, L., Fiterman, D.J., Gal-Gombos, E., Whitman, G., Rouzier, R., et al.: Change in tumor cellularity of breast carcinoma after neoadjuvant chemotherapy as a variable in the pathologic assessment of response. *Cancer: Interdisciplinary International Journal of the American Cancer Society* **100**(7), 1365–1373 (2004)

15. Roux, L.: Mitosis atypia 14 grand challenge (2014), <https://mitos-atypia-14.grand-challenge.org/>
16. Shao, Z., Bian, H., Chen, Y., Wang, Y., Zhang, J., Ji, X., et al.: Transmil: Transformer based correlated multiple instance learning for whole slide image classification. *Advances in neural information processing systems* **34**, 2136–2147 (2021)
17. Tomczak, K., Czerwińska, P., Wiznerowicz, M.: Review the cancer genome atlas (tcga): an immeasurable source of knowledge. *Contemporary Oncology/Współczesna Onkologia* **2015**(1), 68–77 (2015)
18. Xu, F., Zhu, C., Tang, W., Wang, Y., Zhang, Y., Li, J., Jiang, H., Shi, Z., Liu, J., Jin, M.: Predicting axillary lymph node metastasis in early breast cancer using deep learning on primary tumor biopsy slides. *Frontiers in Oncology* p. 4133 (2021)
19. Xu, H., Usuyama, N., Bagga, J., Zhang, S., Rao, R., Naumann, T., Wong, C., Gero, Z., González, J., Gu, Y., et al.: A whole-slide foundation model for digital pathology from real-world data. *Nature* **630**(8015), 181–188 (2024)
20. Yan, R., Shen, Y., Zhang, X., Xu, P., Wang, J., Li, J., Ren, F., Ye, D., Zhou, S.K.: Histopathological bladder cancer gene mutation prediction with hierarchical deep multiple-instance learning. *Medical Image Analysis* **87**, 102824 (2023)
21. Yang, S., Wang, Y., Chen, H.: Mambamil: Enhancing long sequence modeling with sequence reordering in computational pathology. In: *International Conference on Medical Image Computing and Computer-Assisted Intervention*. pp. 296–306. Springer (2024)